PNAS

Main Manuscript for

The oxygen paradox in alkaline zinc-air battery *via* the competition of an unidentified anodic chemical reduction with cathodic kinetics

Subhra R. Pattanayak, Pallavi Thakur, and Tharangattu N. Narayanan

Tata Institute of Fundamental Research Hyderabad, Serilingampally Mandal, Hyderabad 500046, India.

*Tharangattu N. Narayanan

Email: tnn@tifrh.res.in

Author Contributions: S.R.P. identified the process and developed the concept with P.T and T.N.N. S.R.P. conducted the experiments in the supervision of T.N.N. All the authors discussed the results and wrote the manuscript together.

Competing Interest Statement: There is no competing interest.

Classification: Physical Sciences; Chemistry.

Keywords: Superoxide Radical Anion; Chemical Oxygen Reduction; Zinc-O_2 Battery; Electron Paramagnetic Resonance; Hydrogen Evolution Reaction.

This PDF file includes:

Main Text
Figures 1 to 5

Abstract

Can the fuel in use adversely affect the performance of an energy storage system? Here, oxygen (O_2) in zinc-air (O_2) battery (ZAB) is shown to impact the anodic process adversely, leading to early cell failure, though its amount limiting can affect the cathodic reaction kinetics. An unexplored chemical reduction process of dissolved O_2 on metallic zinc in alkaline medium leading to peroxide radical ($O_2^{\bullet -}$) species generation is proven, by electron paramagnetic resonance spectroscopy (EPR) and hydrodynamic voltammetry studies, followed by the formation of ZnO passivation layer on the Zn surface causing cell death. Keeping similar discharge times, early ZnO passivation occurred on the ZAB with its anode kept in an O_2 rich environment than in the other one of O_2 free environment. A slight modification in the cell design ensuring the limited availability of O_2 at anode provided ~5 times extended cyclability (~7 hours to ~35 hours) than the ZAB with no such control leading to enhanced specific capacity. This study unravels an unidentified but major parasitic chemical process by O_2 on the Zn surface, highlighting the importance of cathodic O_2 crossover inhibition in the ZAB.

Significance Statement

Alkaline ZABs are proposed for applications ranging from portable hearing aids to mini-grids, with self-discharge from the hydrogen evolution reaction (HER) on metallic Zn as a major roadblock. However, a new parasitic process has been identified: the chemical reduction of dissolved oxygen (O_2) on Zn surface generates superoxide radical anions, becoming more critical issue than the HER by causing surface modification leading to passivation. This reduction does not occur in metals like iron (Fe) used in alkaline iron-air battery. Presence of O_2 in the anodic compartment leads to early cell failure from passivating ZnO formation impeding charge transfer. Limiting the O_2 transfer from the cathodic side to anodic compartment can extend the cell cyclability and enhance discharge capacity.

Main Text

Introduction

Metal-air (O_2) batteries, owing to their high theoretical energy densities in comparison to metal ion batteries, are emerging as potential plausible energy storage solutions.(1, 2) Out of different metals (Li, Zn, Al, Fe *etc.*) based rechargeable metal-air battery systems, Zn based energy

storage systems find a niche and are considered for futuristic applications as secondary battery due to safety, cost efficiency, widespread abundance, and environmental compatibility along with higher energy density.(3–5) Apart from the higher safety aspects of metallic Zn, the use of aqueous electrolytes – alkaline or neutral, in the system brings additional safety feature to the Zn-air battery (ZAB) unlike that in the Li-air batteries. (6) ZABs are the potentially proven metal-air battery systems in small scale energy storage to grid level storage, and their primary batteries are largely being used in hearing aids. (7) It holds strong promise for future electric vehicles as well as in mini power grids to store intermittent renewable energy.(3, 8–10)

Despite the merits, commercial development of ZAB systems still remains a bottleneck due to some of the following issues: (a) challenges in the development of a bifunctional electrocatalyst for cathode to facilitate the oxygen evolution reaction (OER, during the charging of the battery) and oxygen reduction reaction (ORR, during the discharge of the battery),(11) (b) early passivation of Zn anode due to thick ZnO formation causing cell death,(12) (c) parasitic reactions leading to low coulombic efficiency, self-discharge, and cell malfunctioning.(13, 14) Significant progress has been made during the past few years on the development of bifunctional electrocatalysts for ORR and OER, leading towards the realization of low-cost, durable porous cathodes (15–17). In the anodic side (Zn), early ZnO passivation, *dead* dendrite formation, and parasitic chemical reactions are identified as the critical issues to be addressed. The strategies such as electrolyte modification, electrode structure engineering, anode composition modification, deployment of solid-state electrolyte *etc.* have been suggested as the solutions to address the early cell death, low columbic efficiency, and self-discharge.(18–23) Although the sluggish cathodic kinetics is known to play the rate limiting role in a ZAB, however at higher current densities, both anodic and cathodic processes determine the cell life of ZAB.(24)

In an alkaline ZAB, metallic Zn is in contact with alkaline electrolyte, and it can lead to a chemical reaction forming H_2. This inevitable process leads to the corrosion of Zn and reduction in the columbic efficiency of a conventional ZAB.(25) Similarly other side reactions such as, the role of purity of air supplied at the cathode has also been investigated. It was shown that CO_2 in the air can affect the battery performance due to the formation of soluble and insoluble carbonate and bicarbonate ions.(26) However, O_2 in the air is the reactant supplied at the cathodic side of a ZAB (fuel for the ORR process) and it is soluble (10^{-3} – 10^{-4} mol/L) in alkaline solution.(27) Limiting the amount of O_2 at the cathode leads to a higher over potential in the battery discharging process and hence O_2 mass transfer is critical at cathode (as proven in the later part). Herein we probe the influence of O_2 (g) or dissolved O_2 on the anodic side of a ZAB or Zn-O_2 battery, revealing the possibilities of parasitic reactions other than the well explored hydrogen evolution reaction (HER). Our experiments reveal that an O_2 deficient anodic environment can enhance the H_2 production

along with a prolonged discharge time. It has also been witnessed that gaseous byproducts of chemical reactions occurring in electrochemical systems can be utilized for renewable energy generation.(28) A possible idea made by the authors here is the utilization of generated H_2(g) while exploiting the cell for maximum discharge capacity (discharge time in a given mass of Zn).

Results and Discussion

Effects of O_2 supply in the anodic and cathodic processes of Zn-O_2 battery.

To investigate the role of O_2 at the anodic process, a Zn-Zn symmetric cell is devised (split cell setup is given in *SI Appendix,* Fig. S1a). Zinc metal discs (1 cm diameter) are used as both, the working and counter electrodes, and 6 M KOH as the electrolyte. Cyclic voltammogram (CV) are acquired in N_2 and O_2 supplied environments (fixed flow rate, Fig. *1 A* and *1 B*) (comparison to Ar in *SI Appendix,* Fig. S1b and S1c). For the CV, the potential is swept from -0.4 V to 0.4 V at a scan rate of 1 mV/s. During the positive sweep, the current first increased rapidly, reaching a maximum indicating the Zn to ZnO conversion. Once the Zn surface gets passivated completely with ZnO, the current immediately drops. During the reverse scan, the ZnO layer gets cracks which causes sudden jump in the current.(21) The observed reduction current is due to ZnO to Zn conversion. Though the oxidative and reductive current values are comparable in the initial (say in 5th, Fig. *1 A*) cycles, both gradually decrease with the cycle number in O_2 environment when compared to that in N_2 (O_2 free environment). Similar trend, like in N_2, is also observed with Ar, *SI Appendix,* Fig. S1b and S1c. This symmetric cell study indicates that the Zn surface is becoming electrochemically inactive (passivating) at a much higher rate in the O_2 environment compared to the N_2 and Ar environments.

To investigate whether this deterring effect has any influence in Zn-O_2 full cell performance, charge-discharge experiments are conducted at a constant current density of 5 mA/cm² using a split-cell setup having Zn as an anode, 20 weight % Pt/C coated porous carbon paper as a cathode and 6 M KOH as the electrolyte. One set of the experiment is conducted with a continuous supply of pure O_2 in the cell *via* the cathodic inlet at a constant flow rate while the other set is performed with a mixture of N_2 and O_2 gases (80% N_2, 20% O_2) named as 'air', the schematic is shown in Fig. *1 C* (inset shows oxygen transfer from cathode to anode). The charge-discharge plots are shown in Fig. *1 D*, indicating a nearly five-fold increase in the cyclability in the air environment compared to that in the O_2 environment. The drastic voltage drop after cycling impedes further charging and is identified due to the insulating ZnO formation, as shown in our previous studies. The observed higher overpotential during discharge for the cell running in air-

environment (Fig. *1 D*) is due to the sluggish ORR because of the O_2 mass transfer limitation in the cathodic process, as proven in the later part. However, there is a pronounced influence on the cyclability of the cell, where it reaches up to ~60 hours in the case of air while the cell failure occurs in~12 hours in O_2 supplied one. To test the role of N_2, the experiments are also conducted in an Ar diluted O_2 mixture where cyclability enhancement and overpotential losses are observed (*SI Appendix,* Fig. S2). This indicates that the presence of O_2 influences both, cathodic and anodic processes where its role in anodic process is not unraveled so far.

Hence, in order to avoid the limited O_2 availability at the cathode and study the role of O_2 at the anodic process, the further charge-discharge and full discharge studies are conducted in a customized decoupled split cell where anodic and cathodic sides are separated using an anion (hydroxide) exchange membrane (FAS-50), Fig. *1 E* (inset shows blockage of oxygen transfer from cathode to anode only permeating OH^- ion). Separate gas inlet and outlet are made for both the cathodic and anodic sides. The decoupled split cell locks the supplied gas environment on each side without affecting the other. Hence, the further experiments are performed by varying the anodic environment (O_2 and N_2) while keeping a constant O_2 supply at the cathode. The galvanostatic charge-discharge cyclability at a current density of 5 mA/cm², is shown in Fig. *1 F*. The comparison plot shows an enhanced cyclability (~5-fold from ~5 hours to ~35 hours) in the N_2 environment in comparison to the O_2. The similar charge/discharge overpotentials in both the cases (inset Fig. *1 F*) indicates that the overpotential enhancement observed in Fig. *1 D* is due to the mass transfer limited ORR kinetics at the cathode in diluted O_2 environment. The enhanced ZAB cyclability in O_2 deficient environments in comparison to O_2 rich environments is in accordance with the CV Zn-Zn symmetric cell studies, Fig. *1 A and 1 B*. This indicates the negative influence of the O_2 gas (present in the cell) on the zinc anode reversibility.

Furthermore, the effect of O_2 in early passivation of the Zn (Fig. *2 A*) is also reflected by full-discharge study of the cell. The cells are completely discharged at a current density of 5 mA/cm^2 by varying anodic environment as N_2 and O_2, keeping the cathodic feed same as O_2. The first discharge plot, Fig. *2 B*, indicates an approximately sevenfold increase in the discharge time with anodic N_2 in comparison to that of O_2. This indicates an extended time taken for Zn passivation in presence of N_2, whereas a complete passivation of Zn surface (with ZnO) in O_2 leading to the early cell failure. Moreover, to test the negative influence of O_2 in the discharge capacity retention of the cell, firstly, the cells are fully discharged in different gaseous environment [N_2 (Fig. *2 C*), O_2 (Fig. *2 E*)] followed by the charging for the same time period and repeated for several cycles until the anode is completely passivated and failed. From the data (Fig. *2 D*, Fig. *2 F*), it is inferred that the discharge capacity is retained by nearly 40 % for the second cycle in the N_2 environment in comparison to mere 8 % in the O_2 environment. The trend remains the same with a 22 %, 5 %,

and 3 % capacity retention in the consecutive cycles for the N_2 environment compared to the negligible retention of 1 %, 0.3 %, and 0.1 % respectively, in the O_2 environment. This shows the nature of the ZnO formed is more passivating in the O_2 environment than in the N_2 that results in almost 5 times low discharge capacity even in the second discharge. The discharge capacity of the cell having N_2 supply is found to be higher than that of the O_2 indicating the significant reversibility of the reaction ($Zn + 4\ OH^- \rightarrow [Zn(OH)_4]^{2-} + 2\ e^-$) in the former.

To further investigate the difference in the morphology evolution of the Zn surface during the discharge process in different gas environments, discharge experiments are conducted by controlling at different intervals (Fig. *3 A*) and the respective Zn electrodes are characterized using field emission scanning electron microscopy (FESEM). Herein, five sets of Zn electrodes, discharged up to different intervals (t = 30 mins, 2 h, 5 h, 6 h and 7.5 h i.e. failed) in N_2 supplied electrolytes, are analyzed using FESEM imaging. As shown in Fig. *3 B to 3 F*, a slow evolution of dendritic oxides (ZnO, as verified in the later part) is evident from the initial stage of nodular to flaky and again to nodular oxides. Similarly, electrodes with O_2 supplied condition are also analyzed at different discharge time intervals (t =s, 30 mins, and 50 mins i.e. failed) as shown in 20 min Fig. *3 G to 3 I* (detailed data in *SI Appendix,* Fig. S3). Zinc electrodes, during the discharge in O_2 environment, is led to early passivation and has dominant dendritic features even in the initial stages. The vigorous dendritic growth can be correlated to the early passivation and the formation of irreversible ZnO.

To probe further into the early passivation of zinc, X-ray diffraction (XRD) studies are conducted with Zn electrodes discharged for the same capacity (2.5 mAh/cm^2) i.e. 30 minutes at a current density of 5 mA/cm^2, in the anodic O_2 and N_2 environments. As shown in Fig. *4 A*, the XRD patterns suggest the presence of metallic Zn (ICDD file number 04-0831) having diffraction peaks at 36.3, 39, 43.2, 54.4, 70.1 and 70.7 º corresponding to (002), (100), (101), (102), (103), and (110) planes, respectively, of hexagonal close packing structure in both the electrodes. Along with that, the diffraction peaks at 31.8, 34.5, 36.3, 45.9, 47.6, 56.7, 62.9 º corresponding to (100), (002), (101), (102), (110), (103), and (112) planes, respectively, of wurtzite ZnO (ICDD file number 36-1451) are also present in both the samples indicating a similar phase of ZnO formed in both the environments. However, it is observed that the ratio of the highest intensity peak of ZnO (002) to the metallic Zn (101) is higher (~0.24) in O_2 supplied Zn electrodes than that in the N_2 influenced one (~0.06). This indicates that the increased oxygen pressure enhances the stoichiometry of ZnO by promoting growth along the c-axis. The decrease in full width and half maximum (FWHM) or the sharpening of the (002) peak suggest that the O_2 rich environment leads to the formation of more crystalline ZnO, contributing to the development of a passivating

layer.(29) The XRD studies are also conducted for Zn electrodes discharged at different time intervals of N_2 and O_2 environments, *SI Appendix,* Fig. S4 and S5.

The nature of the 30 minutes discharged electrodes is further investigated using X-ray Photoelectron Spectroscopy (XPS) technique. The XPS survey spectra for both samples show ZnO as the observable phase on the Zn surface (*SI Appendix,* Fig. S6). The high-resolution O 1s spectra are compared for the Zn electrode discharged in N_2, the single peak at binding energy of 531.5 eV corresponds to O 1s of defective or amorphous ZnO (Zn-OH, chemisorbed hydroxyl) as mentioned in the literature(30), the high-resolution spectra of Zn 2p shows the peaks at binding energies of 1021.7 and 1044.8 eV are associated with 2p1/2 and 2p3/2 of Zn in ZnO. Whereas, for the Zn discharged in O_2, two peaks at binding energies of 529.9 and 531.4 eV are observed that correspond to Zn-O and Zn-OH, respectively(31), the high-resolution spectra of Zn 2p shows the peaks at binding energies of 1021.3 and 1044.4 eV are associated with 2p1/2 and 2p3/2 of Zn in ZnO and shifted to lower binding energy than in N_2 environment indicating crystallinity of the formed ZnO.(29) The presence of defect free ZnO in the O_2-influenced zinc indicates a higher degree of passivation and concern for reversibility. This is in correlation with SEM studies that shows the early-dendrite formation in the presence of O_2. XPS analyses of the failed Zn electrodes are discussed in *SI Appendix,* Fig.S4 and S5. The XRD patterns suggest the presence of metallic Zn (ICDD number 04-0831) of hexagonal close packing structure and wurtzite ZnO (ICDD file number 36-1451) phases. Peaks at 30.7, 45.9º correspond to (220), (107) planes of β-$Zn(OH)_2$ (ICDD file number 41-1359). XPS data (*SI Appendix,* Fig.S7) indicates that the O_2 failed sample predominantly forms ZnO, while the N_2 failed sample forms ZnO and some amount of $Zn(OH)_2$. This is also evident that, the corrosion process (by HER) has resulted in $Zn(OH)_2$ formation in alkaline ZABs which seems more prominent in N_2 failed sample (further proved by inline-gas chromatography).

O_2 reduction process on Zn surface leading to ZnO formation.

ZnO is known as a potential catalyst for electrochemical ORR process.(32–34) It has been hypothesized by Pilbath and Sziraki that spontaneous chemical reduction of O_2 can happen on a defective $ZnO/Zn(OH)_2$ surface having excess Zn in the form of interstitial defects leading to a space charge layer at its surface.(35) Hence, metallic Zn can act as electron donor and O_2 can get physiosorbed or chemisorbed on its surface. Moreover, from *ab initio* DFT calculations, the adsorption of O_2 on the ZnO surface is predicted to be facilitated by charge transfer due to excess charge present on the polar surface of ZnO, leading to the formation of chemical bond.(36) Although such predictions exist, a clear understanding is lacking. To understand this passivating ZnO formation is the electrochemical effect, or this is a chemical process occurring on the zinc

surface (the facilitation of ZnO formation) Raman spectroscopy was performed using a 532 nm wavelength light source. 50 mg of Zn powder is dispersed in 50 µL of 1 M KOH. The dispersion is divided into two parts which are kept in O_2 and N_2 environments. The rapid growth of ZnO on the Zn surface kept in alkaline solution, in the presence of O_2, is confirmed by Raman spectroscopy analysis, Fig. *5 A*. From the obtained data, it can be noticed that, there are peaks at 330, 407, 425 and 557 cm^{-1} corresponding to E_{2H}-E_{2L}, E_1 (TO), E_{2H}, and A_1 (LO), respectively.(37–40) The peak at 330 cm^{-1} corresponds to E_{2H}-E_{2L} which has predominately A1 symmetry.(37) The phonon mode at 407 cm^{-1} corresponds to E_1 (TO) is the characteristic wurtzite ZnO.(38) The most distinct and intense peak at around 425 cm^{-1} corresponds to the nonpolar high-frequency optical phonon E_2 mode (E_{2H}), which is associated with oxygen movement and is characteristic of the wurtzite structure, and the red shift in frequency is due to structural defects in the ZnO.(39) The dominant Raman peak around ~560 cm^{-1}, attributed to the surface optical (SO) phonon mode of ZnO, indicates interfacial defects and disorder.(40) These peaks are characteristic peaks of defective ZnO that are very prominent in O_2 environment. This indicates that ZnO phase predominantly develops in O_2 atmosphere in comparison to the N_2 indicating the O_2 undergoing reduction and facilitating the ZnO formation.

To further understand the role of O_2 in a ZAB setup, electrochemical impedance spectroscopy (EIS) measurements are conducted at the open circuit potential (OCP) using a sine wave signal of 10 mV amplitude and within a frequency range of 100 kHz to 1 Hz in N_2 as well as in O_2 environments in alkaline medium. The Nyquist plots given in Fig. *5 B* show semicircular loops, indicating a charge transfer process or the corrosion process, as mentioned in literature.(41)The best fitted Randles' circuit is shown in the inset corresponding to specific adsorption of ionic species at the surface, where their presence is proven in the later part. Here, the R_s represents the ohmic resistance, related to uncompensated contact and electrolyte resistance, R_{ct} denotes the anodic charge-transfer resistance, while Q_d represents the double-layer capacitance. R_f and Q_f correspond to the resistance and capacitance of the ZnO film on the metal surface.(41)The charge transfer resistance value is seen to be 513 Ω in O_2 whereas it is found to be 3428 Ω in N_2 environment, indicating a charge transfer process on Zn surface in presence of O_2.

To further confirm the nature of the chemical species forming in the process, rotating ring disk electrode (RRDE) based experiments are conducted with Zn as the disc electrode, Pt as the outer (ring) electrode, Ag/AgCl (sat.) as a reference electrode, platinum mesh as the counter electrode, and 1 M KOH as electrolyte. Schematic of the O_2 reduction process on the Zn surface in RRDE set up is given in Fig. *5 C*. The disc electrode is kept at the OCP, where the OCP was found to be ~-1.6 V in the N_2 supplied system while the OCP is decreased to -1.5 V with the O_2 supply. The rotation speed is kept constant at 1600 rpm. The Pt ring is set at a potential of 0.5 V

vs Ag/AgCl (sat. KCl) to oxidize the species formed at the disc electrode, if any. The experimental setup is given in *SI Appendix,* Fig. S8A. It is important to note that a notable ring current is observed in O_2 in comparison to that in the N_2 supplied system, as shown in Fig. *5 D*. This suggests the formation of reduced O_2 species (radicals or anions) at the disc electrode when the supplied O_2 encounters the zinc. Negligible ring or disc current are observed when bare glassy carbon disc electrodes or iron powder (another transition metal where its rechargeable alkaline batteries are demonstrated) are taken onto the disc keeping all the other conditions the same (*SI Appendix,* Fig. S8B). This confirms the unique reduction process of O_2 molecules happening at the zinc surface.

Detection of O_2 radicals formed *via* O_2 reduction process on Zn surface.

To confirm the nature of the reduced species formed on the Zn surface (as observed by RRDE experiment), electron paramagnetic resonance (EPR) spectroscopy study is carried out. A 5-membered cyclic nitrone called DMPO (5, 5-Dimethyl-1-Pyrroline-N-Oxide) is a widely used radical trapping agent, that interacts with oxygen radicals to produce nitroxide spin adduct.(42) The sextet signal obtained in EPR (Fig. *5 E*) illustrates the reaction of DMPO with the peroxide radical, resulting in the formation of the adduct, DMPO-$O_2^{\cdot -}$ (Fig. *5 F*). This multiplet in EPR arises from the interaction between the unpaired electron spins and nearby magnetic nuclei, leading to hyperfine splitting (2I+1, where I represent the nuclear spin value). In this case, sextet is the resultant hyperfine splitting due to interaction between two kinds of nuclei [Nitrogen (N) atom (I=1) and hydrogen (H) atom (I=1/2)]. The N nucleus results in 3 lines [coupling constant a(N), 1.83 mT] and each of them splits into two lines due to the H atom presence in β position. [a(β-H), 1.58 mT] resulting in a sextet signal (Fig. *5 G*). This EPR spectra confirms the presence of peroxide radical which clearly indicates the reduction of O_2 on zinc. Hence, O_2 is susceptible to take electron/s from the Zn surface in alkaline solution to form the superoxide radical anions.

Tuning the HER: N_2 vs O_2 gas effects.

The metallic zinc in alkaline condition undergoes self-discharge process due to corrosion reaction because zinc is thermodynamically unstable in concentrated KOH. Under standard conditions with pH of KOH solution 14, the reversible potential for the anode reaction is about −1.26 V *vs* SHE. Meanwhile, the hydrogen evolution reaction has a reversible potential of approximately −0.83 V *vs* SHE. So, corrosion reaction is spontaneously favored (ΔG = -ve) for the alkaline ZAB.

$$2\ H_2O + 2\ e^- \rightarrow H_2 + 2\ OH^- \qquad \ldots (1)$$

$$Zn + H_2O \rightarrow ZnO + H_2 \qquad \ldots (2)$$

Hence, H_2O reacts electrochemically to Zn or itself can undergo electrolysis to form H_2 that leads to corrosion product formation. The corrosion of zinc not only consumes Zn, reducing cell capacity, but can also lead to surface passivation the corrosion products reach the zincate saturation concentration. (43, 44) As surface sites are used for the HER process, its change was monitored in O_2 and N_2 supplied environments. The differences in the formation of H_2 is studied using inline gas chromatography (GC) measurements connected to the anode compartment during the discharge of the battery.

The GC study indicates significant differences in the amount of H_2 produced in presence of O_2 and N_2 supplied anodic processes. H_2 production is monitored in 20 minutes intervals. Upon assembling, the cell is left at OCP condition with N_2 and O_2 supply in two different sets (*SI Appendix,* Fig. S9A). The amount of H_2 detected is higher in the N_2 environment than in the O_2 environment, as H_2 detection is the result of parasitic corrosion reaction occurring on the Zn surface and initial defects propagate corrosion more easily. In the presence of O_2, the parasitic ORR initiates defects on Zn surface that results in more corrosion on Zn surface initially but with the time, the parasitic ORR results in the surface passivation as noticed from decreased cell OCP from 1.42 V to 1.14 V within 90 minutes, whereas minute decrease in OCP (1.41 V) was observed in N_2 rich condition. Even when the cell is discharged at higher current densities of 5 mA cm^{-2}, the observed H_2 production in GC (Fig. *5 H*) is higher in the presence of N_2 than that in the O_2. It has been observed that H_2 formation remains significantly higher in the N_2 while it diminishes consistently in O_2 as the cell goes towards the failure and reaches to 0 ppm as the cell failed completely in O_2 due to complete passivation. It is also observed that switching the supplied gas from N_2 to O_2 rapidly reduces the amount of H_2. In the O_2 environment, some of the surface sites undergo side reactions with oxygen, as mentioned before, resulting in less sites available for HER. After the O_2 supply, while the further backing of N_2 doesn't retrieve the H_2 formation (*SI Appendix,* Fig. S9B). It is evident from here that the more active Zn surface is exposed in anodic N_2 supplied environment. Hence, in the presence of O_2 gas, ORR and HER appear as the side reactions of the ZAB. However, by eliminating the O_2 reaching at the anode surface, HER stays as the dominant side reaction. This also indicates that O_2 reduction is the major parasitic process in the alkaline ZAB than HER. Effective reduction of ORR process in ZAB by protecting the Zn surface can prolong the cell cyclability and energy density (capacity * voltage).

Conclusion

In conclusion, chemical oxygen reduction reaction is identified as the major parasitic process leading to the self-discharge of an alkaline zinc-air battery (ZAB) - one of the high energy density electrochemical storage systems having self-discharge as the main obstacle in their commercial

implementation.(45) Superoxide radical formation from dissolved O_2 is found to be occurring on alkaline Zn surface (Fig. *5 I*) leading to the early failure of the ZAB by passivating ZnO formation. Presence of O_2 is critical in the kinetics of cathodic processes of ZAB where its limited supply can cause high overpotentials. It is shown here that the dissolved O_2 can affect the Zn anode adversely and by limiting the O_2 presence in anode can enhance the discharge capacity and cell cyclability (~35 hours) ~5 times than that devoid of such control (~7 hours). It is also proven that the amount of H_2 produced *via* the inevitable HER process is enhanced with the limited supply of O_2 at the anode. This signifies a higher amount of available active metallic Zn for the discharge process leading to the possibilities of ZABs having high energy density, cell cyclability.

Materials and Methods

Materials.

Zinc foil (0.25 mm thick, 99.98%) was purchased from Alfa Aesar. A gas diffusion electrode platinum–carbon (Pt/C)-coated carbon paper was purchased from Sainergy Fuel Cell India Pvt. Ltd. Whatman Glass microfiber filter paper used as separators was purchased from GE Healthcare Life Sciences. Potassium hydroxide (KOH, 85% extra pure was purchased from Sisco Research Laboratories Pvt. Ltd. Fumasep FAS-50 anion exchange membrane was purchased from Fuel cell store. Pvt. Ltd.

Methods.

Methods include ZAB Cell Design, Electrochemical and Battery Measurements, Surface Characterization Techniques, Gas Chromatography and EPR Measurements, and are provided in *SI Appendix, Experimental details.*

Acknowledgments

Tata Institute of Fundamental Research Hyderabad (TIFR) acknowledge the support of the Department of Atomic Energy, Government of India, under Project Identification No. RTI4007. SRT thanks Mr. Amar Kumar at TIFRH for the fruitful discussion on EPR. Authors thank Ms. Shravani for the SEM and XPS analyses.

References

1. Y. Li, J. Lu, Metal-Air Batteries: Will They Be the Future Electrochemical Energy Storage Device of Choice? *ACS Energy Lett.* **6**, 1370–1377 (2017).

2. J. N. Liu, *et al.*, A brief history of zinc-air batteries: 140 years of epic adventures. *Energy Environ. Sci.* **15**, 114–143 (2022).

3. S. S. Shinde, *et al.*, Ampere-hour-scale zinc–air pouch cells. *Nat. Energy* **6**, 592–604 (2021).

4. X. Fu, *et al.*, Direct solar energy conversion on zinc-air battery. *Proc. Natl. Acad. Sci. U.S.A.* **121**, 123456–123463 (2024).

5. Y. Song, *et al.*, A Hybrid Redox-Mediated Zinc-Air Fuel Cell for Scalable and Sustained Power Generation. *Angew. Chem. Int. Ed.* **63**, 2345–2350 (2024).

6. H. Chen, *et al.*, High-Performance Neutral Zinc-Air Batteries Based on Hybrid Zinc/Carbon Nanotube Fiber Anodes. *Adv. Mater. Technol.* **8**, 2200987 (2023).

7. X. Bi, *et al.*, Rechargeable Zinc–Air versus Lithium–Air Battery: from Fundamental Promises Toward Technological Potentials. *Adv. Energy Mater.* **14**, 2301254 (2024).

8. S. S. Shinde, *et al.*, Scaling-Up Insights for Zinc–Air Battery Technologies Realizing Reversible Zinc Anodes. *Adv. Mater.* **35**, 2209722 (2023).

9. X. Zhong, *et al.*, Rechargeable Zinc–Air Batteries with an Ultralarge Discharge Capacity per Cycle and an Ultralong Cycle Life. *Adv. Mater.* **35**, 2300410 (2023).

10. D. Stock, S. Dongmo, J. Janek, D. Schröder, Benchmarking Anode Concepts: The Future of Electrically Rechargeable Zinc-Air Batteries. *ACS Energy Lett.* **4**, 1287–1294 (2019).

11. Y. Song, W. Li, K. Zhang, C. Han, A. Pan, Progress on Bifunctional Carbon-Based Electrocatalysts for Rechargeable Zinc–Air Batteries Based on Voltage Difference Performance. *Adv. Energy Mater.* **14**, 2301381 (2024).

12. W. Xie, K. Zhu, H. Yang, W. Yang, Advancements in Achieving High Reversibility of Zinc Anode for Alkaline Zinc-Based Batteries. *Adv. Mater.* **36**, 2209412 (2023).

13. T. Subramaniam, M. B. Idris, S. K.S., R. K.S., D. S., Mitigating hydrogen evolution reaction and corrosion of zinc in electrically rechargeable zinc-air batteries using nanofluid electrolytes. *J. Energy Storage* **81**, 106783 (2024).

14. J. Yi, *et al.*, Challenges, mitigation strategies and perspectives in development of zinc-electrode materials and fabrication for rechargeable zinc-air batteries. *Energy Environ. Sci*. **11**, 3075–3095 (2018).

15. R. He, *et al.*, A CrMnFeCoNi high entropy alloy boosting oxygen evolution/reduction reactions and zinc-air battery performance. *Energy Storage Mater.* **58**, 111112 (2023).

16. P. Thakur, *et al.*, Cobalt Nanoparticles Dispersed Nitrogen-Doped Graphitic Nanospheres-Based Rechargeable High Performance Zinc-Air Batteries. *ACS Appl. Energy Mater.* **3**, 2122–2130 (2020).

17. Y. P. Deng, *et al.*, Reconstructing 3d-Metal Electrocatalysts through Anionic Evolution in Zinc-Air Batteries. *J. Am. Chem. Soc.* **145**, 8423–8432 (2023).

18. C. Mou, *et al.*, A 3D-printed square-hole electrode for dendrite-free zinc-air batteries. *Inorg. Chem. Front.* **10**, 2052–2061 (2023).

19. W. Xie, K. Zhu, H. Yang, W. Yang, Advancements in Achieving High Reversibility of Zinc Anode for Alkaline Zinc-Based Batteries. *Adv. Mater.* **36**, 2209412 (2023).

20. D. Qiu, *et al.*, A review on zinc electrodes in alkaline electrolyte: Current challenges and optimization strategies. *Energy Storage Mater.* **61**, 103639 (2023).

21. P. Thakur, *et al.*, Extending the Cyclability of Alkaline Zinc-Air Batteries: Synergistic Roles of Li+ and K+ Ions in Electrodics. *ACS Appl. Mater. Interfaces* **13**, 36234–36245 (2021).

22. X. Liu, *et al.*, Mapping the Design of Electrolyte Materials for Electrically Rechargeable Zinc–Air Batteries. *Adv. Mater.* **33**, 2105243 (2021).

23. S. Chen, *et al.*, “Ordered planar plating/stripping enables deep cycling zinc metal batteries” Sci. Adv. **10**, eadn2265 (2024).

24. Investigation of failure mechanism of rechargeable zinc–air batteries with poly (acrylic acid) alkaline gel electrolyte during discharge–charge cycles at different current densities. *Chem. Eng. J.* **429**, 132154 (2022).

25. X. Zhong, *et al.*, Rechargeable Zinc–Air Batteries with an Ultralarge Discharge Capacity per Cycle and an Ultralong Cycle Life. *Advanced. Mater.* **35**, 2300410 (2023).

26. H. Mohammadpour, R. Cord-Ruwisch, A. Pivrikas, G. Ho, Utilisation of oxygen from water electrolysis – Assessment for wastewater treatment and aquaculture. *Chem. Eng. Sci.* **246**, 116875 (2021).

27. S. Zhao, *et al.*, Anti-CO2 strategies for extending Zinc-Air Batteries' Lifetime: A review. *Chem. Eng. J.* **450**, 138785 (2022).

28. R. E. Davis, G. L. Horvath, C. W. Tobias, The solubility and diffusion coefficient of oxygen in potassium hydroxide solutions. *Electrochim. Acta* **12**, 287–297 (1967).

29. J. He, B. Tan, Y. Su, S. Yang, Q. Wei, XPS analysis of ZnO thin films obtained by pulsed laser deposition. *Adv. Mater. Res*. **586**, 6293–6296 (2012).

30. Z. Wang, et al., Structure and strong ultraviolet emission characteristics of amorphous ZnO films grown by electrophoretic deposition. *J. Appl. Phys*. **93**, 2604–2608 (2003).

31. X. Zhang, et al., Effect of aspect ratio and surface defects on the photocatalytic activity of ZnO nanorods. *Sci. Rep*. **4**, 7393 (2014).

32. A. P. Yadav, A. Nishikata, T. Tsuru, Oxygen reduction mechanism on corroded zinc. *J. Electroanal. Chem*. **585**, 142–149 (2005).

33. S. Nayak, P. U. Biedermann, A. Erbe, Superoxide intermediate in the oxygen reduction on a zinc hydroxide model corrosion product. *J. Chem. Phys*. **157**, 104703 (2022).

34. M. Prestat, et al., Oxygen reduction at electrodeposited ZnO layers in alkaline solution. *Electrochim. Acta* **218**, 228–236 (2016).

35 Z. Pilbáth, L. Sziráki, The electrochemical reduction of oxygen on zinc corrosion films in alkaline solutions. *Electrochim. Acta* **53**, 3218–3230 (2008).

36. A. Castro, S. Calderon, L. Marques, Oxygen adsorption on polar and non-polar Zn heterostructures from first principles. *Materials* **16**, 1221 (2023).

37. S. Kumar, et al., Structural and optical properties of ZnO and ZnO nanoparticles under dense electronic excitations. *J. Appl. Phys*. **114**, 073514 (2013).

38. J. Thyr, L. Österlund, T. Edvinsson, Polarized and non-polarized Raman spectroscopy of ZnO crystals: Method for determination of crystal growth and crystal plane orientation for nanomaterials. *J. Raman Spectrosc*. **52**, 1395–1405 (2021).

39. B. Ouni, T. Larbi, M. Amlouk, Vibrational, electronic, and structural study of sprayed ZnO thin film based on the IR-Raman spectra and DFT calculations. *Cryst. Struct. Theory Appl*. **11**, 23–38 (2022).

40. H. Zeng, X. Ning, X. Li, An insight into defect relaxation in metastable ZnO reflected by a unique luminescence and Raman evolutions. *Phys. Chem. Chem. Phys*. **17**, 19637–19642 (2015).

41. M. H. Lin, C. J. Huang, P. H. Cheng, J. H. Cheng, C. C. Wang, Revealing the effect of polyethylenimine on zinc metal anodes in alkaline electrolyte solution for zinc-air batteries: Mechanism studies of dendrite suppression and corrosion inhibition. *J. Mater. Chem*. A **8**, 20637–20649 (2020).

42. X. He, Y. Luo, Y. Yi, S. Su, W. Qin, Peroxymonosulfate activation by Fe-Mn co-doped biochar for carbamazepine degradation. *RSC Adv.* **14**, 1141–1149 (2024).

43. L. Ren, et al., Suppressing metal corrosion through identification of optimal crystallographic plane for Zn batteries. *Proc. Natl. Acad. Sci. U.S.A*. **121**, 15460–15468 (2024).

44. S. S. Shinde, et al., Scaling-up insights for zinc–air battery technologies realizing reversible zinc anodes. *Adv. Mater*. **35**, 2301477 (2023).

45. Z. P. Cano, et al., Batteries and fuel cells for emerging electric vehicle markets. *Nat. Energy* **3**, 279–289 (2018).

Figures

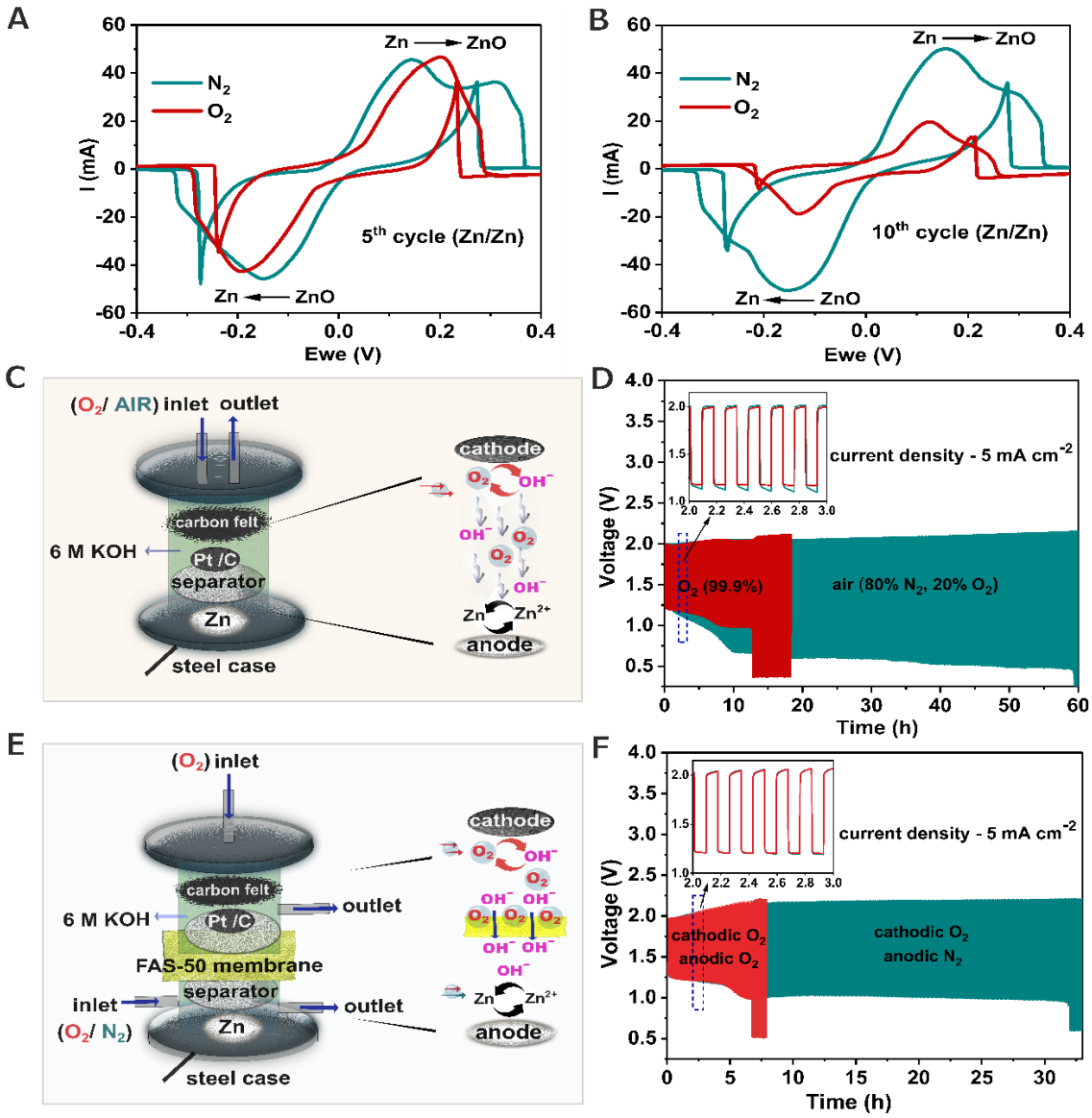

Figure 1. *Zn/Zn symmetric cell performance comparison for (A) 5th and (B) 10th cycles of CV curves in N_2 and O_2, respectively. (C) Schematic of the split cell with components. Zn disc as an anode, a separator, Pt/C as cathode, and carbon felt as gas diffusion layer. Inset shows O_2 transfer to anodic compartment (D) Galvanostatic charge-discharge curves of O_2 vs air. (E) Schematic of a decoupled split cell (two compartments separated by FAS-50 anion exchange membrane) having two set of inlets and outlets in each electrode compartments. Inset shows blockage of O_2 transfer, OH^- anions flow to the anodic compartment (F) Galvanostatic charge-discharge curves of O_2 vs N_2.*

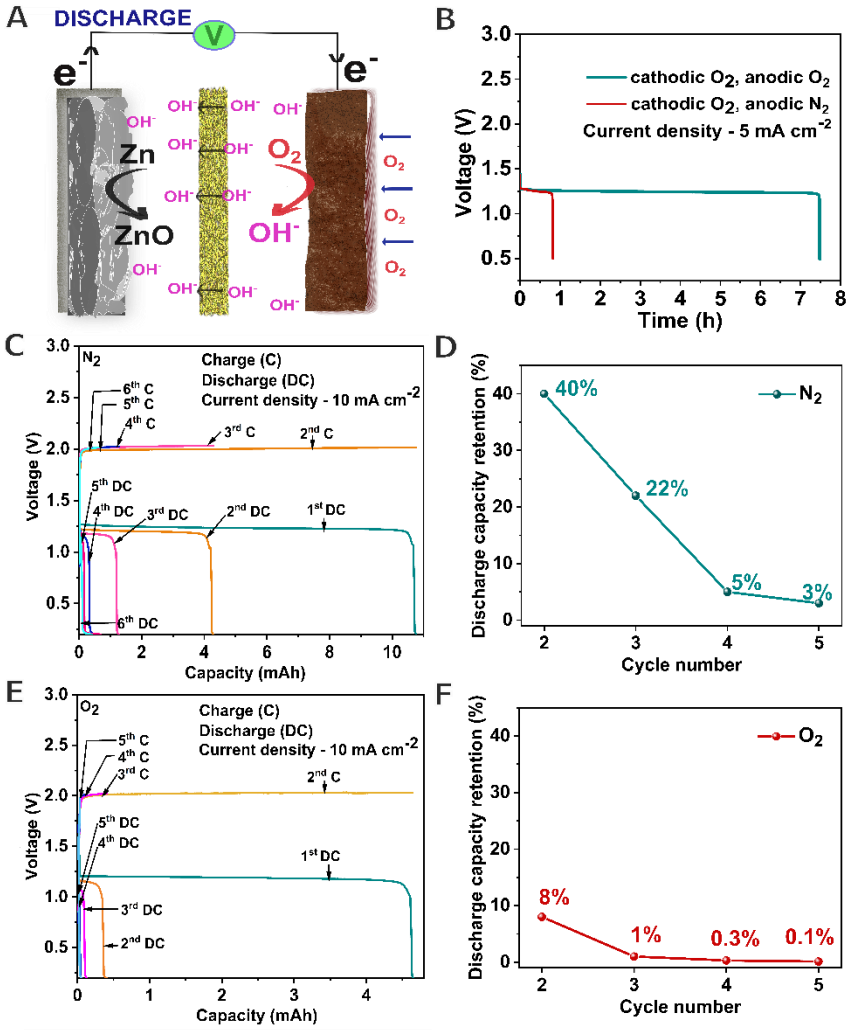

Figure 2. *(A) Schematic of the discharge process in Zn-air (O_2) battery. (B) Full discharge curves of ZAB discharged in O_2 vs. N_2 at 5 mA cm^{-2}. Consecutive full discharge and corresponding charge capacity curves at 10 mA cm^{-2} for (C) in N_2 and (D) the corresponding discharge capacity retention (%) (E) Consecutive full discharge and corresponding charge capacity curves at 10 mA cm^{-2} in O_2 and (F) the corresponding discharge capacity retention (%), indicating overall low capacity and poor capacity retention.*

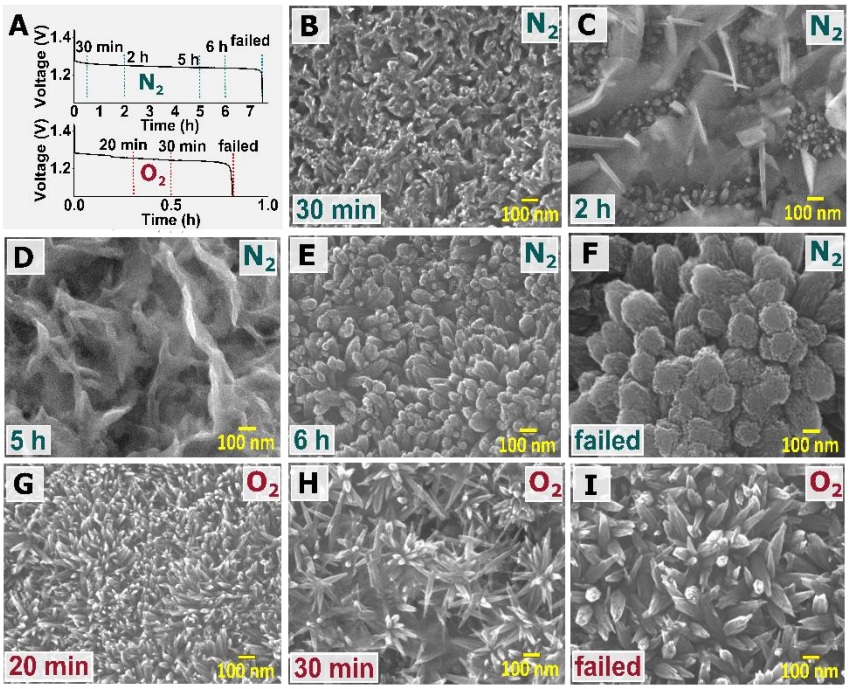

Figure 3. *(A) Different time segments shown during discharge process when Zn is exposed to different gases (N_2 and O_2). FESEM images (scale bars are shown) of Zn electrodes discharged in N_2 at intervals of (B) 30 mins, (C) 2 h, (D) 5 h, (E) 6 h, and (F) failed. The FESEM images of Zn electrodes in O_2 environment discharged for (G) 20 mins, (H) 30 mins, and (I) failed.*

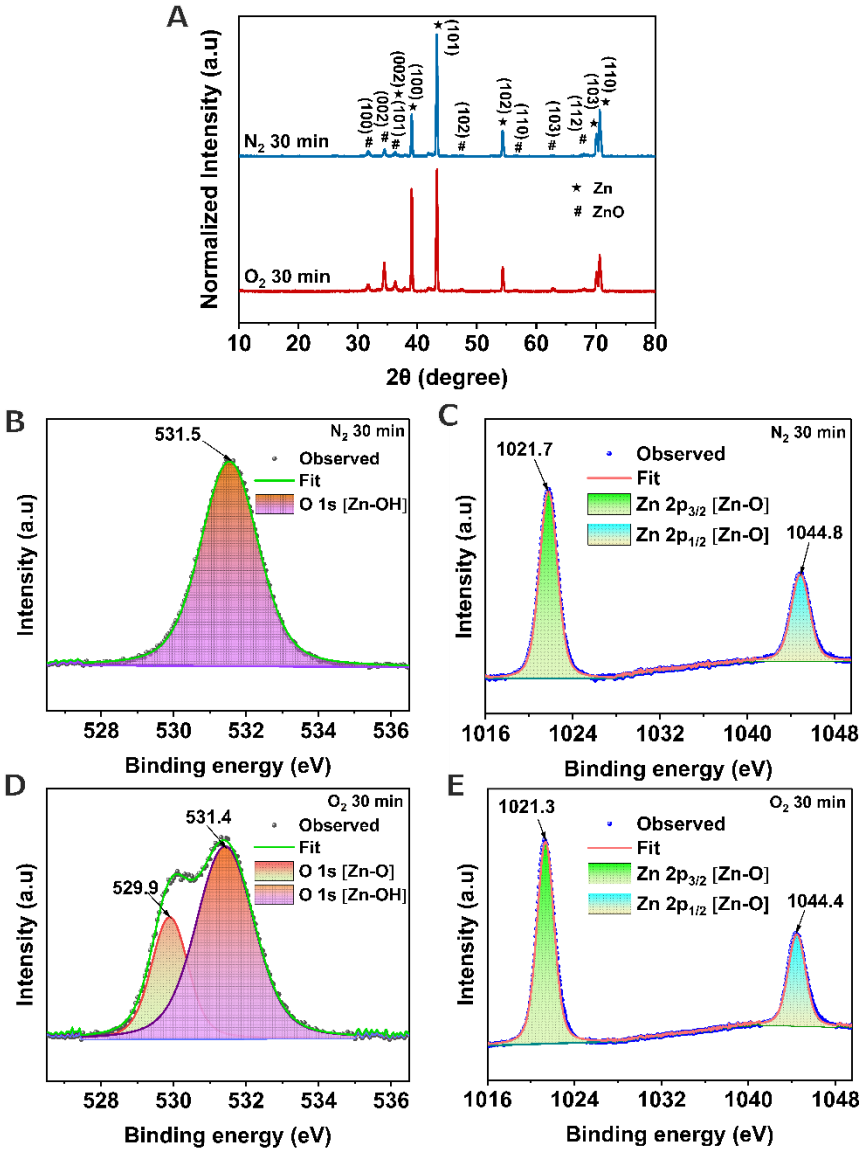

Figure 4. *Bulk and surface characterization of samples discharged for 30 minutes. (A) XRD pattern overlay for zinc electrodes discharged in N_2 vs O_2 for 30 minutes. XPS high resolution spectra for (B) O 1s and (C) Zn $2p_{3/2}$ of zinc discharged in N_2. (D) O 1s (E) Zn $2p_{3/2}$ of zinc discharged in O_2.*

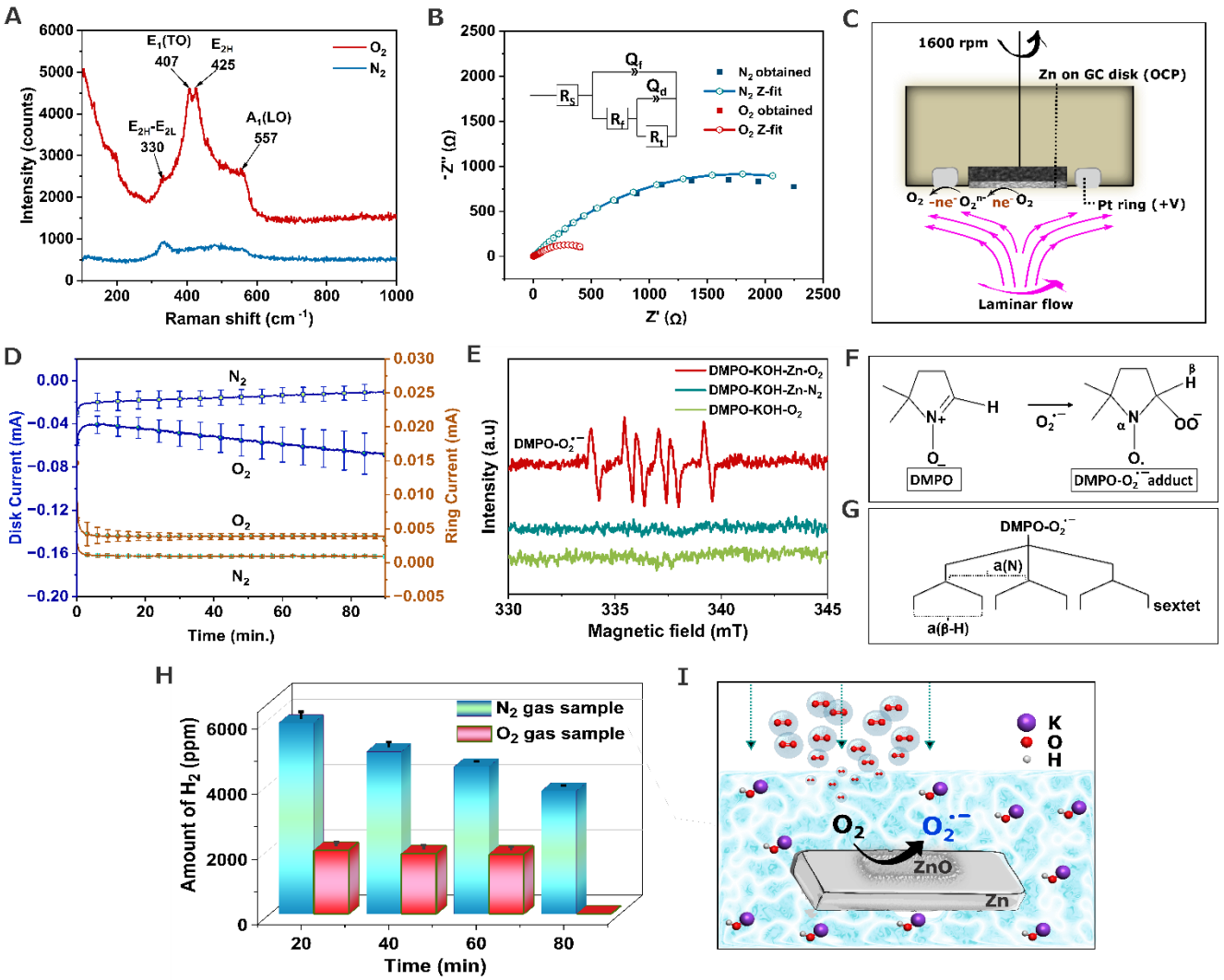

Figure 5. (A) Raman spectra showing A_1 (LO), E_{2H}, E_1 (TO), E_{2H}-E_{2L} modes of ZnO in O_2 environment and only E_{2H}-E_{2L} mode in N_2 environment. (B) The EIS spectra obtained in N_2 and O_2 environments indicating a lower charge transfer resistance in the latter. The best fitted Randles' circuit is shown in the inset. (C) Schematic of the RRDE set up used (without showing the electrical connections) for studying the in situ O_2 reduction process on Zn surface. (D) Disk and ring currents in the presence of N_2 and O_2 gases (standard error bars indicate the deviation in different set of measurements) as marked. (E) EPR analyses showing a sextet spectrum for superoxide anion radical in O_2 and no such characteristic signal in control experiments. (F) Spin trapping of the superoxide radical anion by DMPO. (G) Hyperfine splitting indicating the possibilities of the formation of sextet. (H) Inline-gas chromatography data showing the amount of H_2 produced (with standard error) during cell discharge at 5 mA cm^{-2} in two different gaseous

environments. (I) Schematic illustration of peroxide radical formation in alkaline medium by spontaneous O_2 reduction on Zn surface.